IEEE Access
Multidisciplinary | Rapid Review | Open Access Journal

Received January 2, 2020, accepted January 21, 2020, date of publication January 27, 2020, date of current version February 5, 2020.

Digital Object Identifier 10.1109/ACCESS.2020.2969546

Three-Phase Series Resonant DC-DC Boost Converter With Double LLC Resonant Tanks and Variable Frequency Control

MOHAMED SALEM[1], (Member, IEEE), VIGNA K. RAMACHANDARAMURTHY[2], (Senior Member, IEEE), AWANG JUSOH[3], SANJEEVIKUMAR PADMANABAN[4], (Senior Member, IEEE), MOHAMAD KAMAROL[1], (Senior Member, IEEE), JIASHEN TEH[1], (Member, IEEE), AND DAHAMAN ISHAK[1], (Senior Member, IEEE)

[1]School of Electrical and Electronic Engineering, Universiti Sains Malaysia, Nibong Tebal 14300, Malaysia
[2]Department of Electrical Power Engineering, Institute of Power Engineering, College of Engineering, Universiti Tenaga Nasional, Kajang 43000, Malaysia
[3]Faculty of Electrical Engineering, University Technology Malaysia, Johor Bahru 81310, Malaysia
[4]Department of Energy Technology, Aalborg University, 9220 Aalborg, Denmark

Corresponding author: Mohamed Salem (salemm@usm.my)

This work was supported by Universiti Sains Malaysia (USM) through Short Term under Grant 304/PELECT/6315330.

ABSTRACT This paper proposes a three-phase inverter combined with two LLC resonant tanks series resonant DC-DC boost converter with variable frequency control. The three-phase inverter side of the proposed circuit is connected to identical two-level LLC tanks to ensure balanced resonant currents. The proposed converter requires less switching devices and transformers as compared to the conventional interleaved LLC resonant converter, which competitively offers higher efficiency and reduced size and cost. Furthermore, the proposed converter works above the resonant frequency to achieve zero voltage switching (ZVS) for the entire operating frequency range ($42.5kHz < f_s < 50kHz$) for all switches. Variable frequency controller is considered in order to obtain better stability for diverse loads. Therefore, the proposed converter will have the ability to respond to the load changes by varying the switching frequency to the value that fulfils the requirement. In order to verify the improvement of the proposed converter, the converter performance is compared to conventional interleaved LLC resonant converter. The theoretical outcomes are confirmed through simulation studies using MATLAB/SIMULINK and validated experimentally using a laboratory prototype. Selected results are presented to verify the effectiveness of the proposed converter.

INDEX TERMS Series resonant converter, LLC, zero voltage switching, variable frequency control.

I. INTRODUCTION

Due to rapid improvements of modern-clean energy and industrial applications in power electronics, for instance hybrid electric vehicle (HEV), smart grids, renewable energy systems (RES), and solid state transformers, resonant DC-DC converters have earned consequential and essential interests. This can be attributed to their effective features as compared to the conventional converters in order to appease the requirements of the industrial applications of power electronics. Resonant DC-DC converters have efficient power density, capacity to operate at high switching frequency with soft switching realization, high conversion, and noticeable reduction in size of the magnetic components such as transformers and passive filters [1]–[4]. Furthermore, resonant power converters, RPCs, utilize other method to realize soft switching requirements rather than embracing auxiliary equipment for each switch. RPCs structure them in the form of Resonant Tank Network (RTN) with two or three or multi-reactive elements connected in cascade with the converter [5]. Moreover, RTN types could be categorized based on their elements connection methods and the number of the tank

The associate editor coordinating the review of this manuscript and approving it for publication was Yijie Wang.

elements [6]. The Parallel Resonant Converter (PRC) and Series Resonant Converter (SRC) are considered the most popular topologies of the two-element resonant tank network type. While the Series-Parallel Resonant Converter (SPRC) like LLC and LCC are considered under three-elements, and LCLC is a multi-element resonant tank [7]. Besides, the soft switching technique in power resonant converter also relies on the relation between resonant frequency and switching frequency. In cases where the switching frequency is lower than the resonant frequency, the resonant converter will then obtain Zero Current Switching (ZCS) commutation for all switches [8]. In contrary, Zero Voltage Switching (ZVS) can be achieved when the switching frequency is higher than the resonant frequency [4]. Series resonant converters have been implemented in many applications in literature owing to their popularity and simplicity [9], [10], where the LC resonant tank is connected in series with the loaded-rectifier network. Consequently, the drawbacks of the SRC could be highlighted according to the law of the voltage divider where the input voltage is distributed between the resonant impedance and the resistive load, which makes the voltage gain less than unity [5], [11]. Moreover, the achievement of the zero voltage switching is restricted to the input voltage range and specific load conditions. The output voltage cannot be controlled at no-load operation [12], [13].

LLC resonant topologies have been developed to overcome the limitations of SRC, whereby they exhibit high voltage gain, low electromagnetic interference (EMI), wide operating range and efficient conversion [14], [15]. These topologies have been presented for half and full-bridge primary inverter and with either full-bridge or center-tapped rectifiers on secondary side, where the center-tapped rectifiers are not preferred due the high voltage stress on the diodes. The LLC output voltage or current can be regulated in a wide range by varying the switching frequency [16]–[18]. Also, Series Resonant Converter with two series transformers has been proposed in [12] to turn on all switches at ZVS with wide load conditions and input voltage ranges. Despite the fact that, single stage resonant converters are well-entrenched and advanced in many applications, nevertheless they face some challenges in high input voltage applications, where the current stress on switches devices cause a reduction in both efficiency and reliability [19]. Therefore, this has led to the introduction of multilevel converters, that allows the use of low voltage rating switching devices for high voltage applications [20], [21]. Moreover, the operating modes of three-phase three-level are discussed in [22], where the soft switching range is clearly enlarged when compared to PWM controlled three phase three level converter [23]. On the other hand, multi-phase parallel technique is introduced in [24], but the resonant frequencies were not equal in each individual LLC phase, which caused imbalanced output currents between the phases. Also, authors in [25] have proposed a three-phase interleaved LLC resonant converter that consists of three full-bridge LLC resonant converters with the associated secondary parts are combined using Y-connected diode rectifier which is suitable for high voltage applications with ZVS achievement for all power switches. A hybridization of three-phase and LLC controlled using phase-shift technique is presented in [26] to reduce the conduction losses by sharing the lagging switches between the three-level converter and the LLC converter at the primary side of the transformers, which also reduces the circulating current. Although, LLC series resonant converter has many advantages over conventional topologies, but many output capacitors are needed to deal with output voltage ripples especially in low-voltage and high-current applications. Therefore, a two-phase interleaved LLC converter has been proposed by utilizing a phase of the resonant capacitor and adopting synchronous rectification at secondary side in [27]. As a result, the conduction loss and the output capacitor can be reduced by the interleaved operation.

In this paper, a new combination of three-phase inverter with two LLC resonant tanks series resonant dc-dc boost converter is presented. The proposed converter achieves high output voltage gain with a reduction in the number of power switches and components compared to the conventional three-phase interleaved LLC resonant converter [25], and two-phase common inductor LLC converter [1]. The converter achieves balanced resonant currents by utilizing identical LC tanks, which are linked in series with two step-up transformers to boost the voltage gain and to enhance the ZVS range. The output voltage is regulated by adopting variable frequency control, where the gain of the system is analyzed with respect to the tank impedance, which is a function of the relation between the switching frequency and resonant frequency.

The remaining paper is organized as follows: Section II describes the circuit configuration of the proposed converter and its main characteristics. The various operating modes are explained in Section III. The simulation results are presented in section IV. Selected experimental results using 5 kW scaled laboratory prototype are reported in Section V to validate the theoretical findings. Finally, the work is summarized and concluded in section VI.

II. THE PROPOSED CONVERTER: CIRCUIT TOPOLOGY AND CHARACTERISTICS ANALYSIS

Figure 1 illustrates the schematic diagram of the proposed converter formed by a simple three-phase inverter feeding two LLC resonant tanks, where each tank is performed by resonant inductance L_r, resonant capacitance C_r, and the magnetizing inductance of the HF transformer L_m.

Both HF transformers are connected to each other in series in the secondary side, and are connected to the loaded full-bridge diode rectifier.

A. CIRCUIT CONFIGURATION

The proposed converter structure shown in Fig.1 is different than other reported topologies in the literature [1], [25], as two LLC tanks are connected to the three-phase inverter by sharing the leg B, and both tanks are sharing a full bridge diode rectifier. Thus, this structure will lead to significant

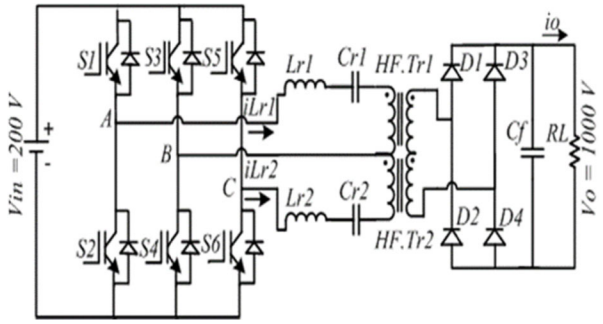

FIGURE 1. Schematic diagram of the proposed three-phase with two LLC tanks series resonant converter.

reduction in the used components and size/weight and cost. Here, it contains three phase inverter rather than two or three level inverters, which confirms the reduction of the proposed converter active switches. Also, the two transformers are connected in series and linked to full bridge rectifier which confirms the reduction of the rectifier diodes when compared to three phase rectifiers. It should be noted that both resonant tanks of the proposed converter are identical (i.e. $L_{r1} = L_{r2}$. and $C_{r1} = C_{r2}$) to ensure balanced resonant tank variables, i.e i_{Lr1}, i_{Lr2}, v_{Cr1}, and v_{Cr2} and to produce equal resonant frequencies to simplify the design considerations. Hence, all inverter switches ($S_1 - S_6$) will be able to achieve ZVS if resonant tanks impedance can behave inductively. Furthermore, each resonant tank will transfer/deliver half of the power to the output load. Also, the aim of utilizing two HF step up transformers is to boost the gain and overcome the limitation of the SRC, where the magnetizing inductance will ensure the achievement of the ZVS for all switches by enhancing the resonant tank inductivity. The primary windings of both transformers are connected to the end of the resonant tanks through the Leg B as shown in Fig. 1 while the secondary windings are connected to each other in series and to the full bridge-rectifier. This will led to the currents balance through the resonant tanks and the secondary side. Furthermore, the boosted output voltage is regulated by utilizing variable frequency control to obtain wide load variation and to achieve soft switching.

B. CIRCUIT CHARACTERISTICS AND ANALYSIS

The line-to-line voltages, V_{AB}, V_{BC} and V_{CA} of the voltage source inverter shown in Fig. 1 that feeds the resonant tanks can be expressed using Fourier series as follows:

$$V_{AB}(t) = \frac{4V_g}{\pi} \sum_{n=1,3,5,\ldots} \frac{1}{n}(\sin(n\omega_s t) - \sin n\left(\omega_s t - \frac{2\pi}{3}\right) \quad (1)$$

$$V_{BC}(t) = \frac{4V_g}{\pi} \sum_{n=1,3,5,\ldots} \frac{1}{n}\left((\sin n\,\omega_s t - \frac{2\pi}{3}) - \sin n\left(\omega_s t - \frac{4\pi}{3}\right)\right) \quad (2)$$

$$V_{CA}(t) = \frac{4V_g}{\pi} \sum_{n=1,3,5,\ldots} \frac{1}{n}\left(\left(\sin n\left(\omega_s t - \frac{4\pi}{3}\right)\right) - (\sin(n\omega_s t))\right) \quad (3)$$

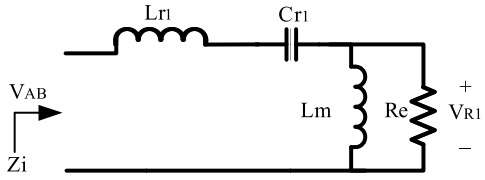

FIGURE 2. The AC equivalent circuit for one of the LLC resonant tanks.

where V_g the peak value of the square-wave of the inverter output voltage and ω_s is the angular switching frequency. The line-to-line voltage contains harmonics of order $2n-1$ (n = integer).

Assume that the voltage V_{AB} is applied to one of the LLC resonant tanks as shown in the equivalent circuit in Fig.2, The AC voltage gain of the LLC resonant tank can be obtained by splitting the voltage between the input and the output impedances. The effective resistance R_e is converted from the secondary to primary part by using the transformer winding ratio, and the converter gain equation can be expressed as the following equations:

$$Z_i = X_{Lr} + X_{Cr} + (X_{Lm}//R_e) \quad (4)$$

$$Z_0 = (X_{Lm}//R_e) \quad (5)$$

$$M = \frac{\frac{V_o}{n}}{V_{AB1}} = \frac{Z_o}{Z_i} = \frac{\frac{j\omega_s L_m . R_e}{R_e + j\omega_s L_m}}{j\omega_s L_r - \frac{j}{\omega_s C_r} + \frac{j\omega_s L_m . R_e}{R_e + j\omega_s L_m}} \quad (6)$$

Equivalently, the voltage gain of the second LLC resonant tank can be obtained with the same manner, as all the tank parameters are identical to the first tank. Hence, the resonant tank parameters can be defined by the following expressions:

$$\text{Resonance frequency}: f_r = \frac{1}{2\pi\sqrt{L_r C_r}} \quad (7)$$

$$\text{Inductance ratio}: A_L = \frac{L_m}{L_r} \quad (8)$$

$$\text{Characteristic impedance}: Z_o = \sqrt{\frac{L_r}{C_r}} = 2\pi f_r L_r = \frac{1}{2\pi f_r C_r} \quad (9)$$

$$\text{Loadquality factor}: Q = \frac{Z_o}{R_e} = \frac{\omega_r L_r}{R_e} = \frac{1}{\omega_r C_r R_e} \quad (10)$$

$$\text{Effective ac resistance}: R_e = \frac{8n^2}{\pi^2} R_L \quad (11)$$

where ω_r is the angular resonant frequency, A_L is the inductance ratio between the resonant inductance L_r, and the magnetizing inductance L_m while, n is the transformer turns ratio, and R_e is the effective equivalent ac resistance consisting of the full rectifier bridge with capacitor and the load.

According to (10), the resonant inductor value can be calculated by:

$$L_r = \frac{QR_e}{\omega_r} \quad (12)$$

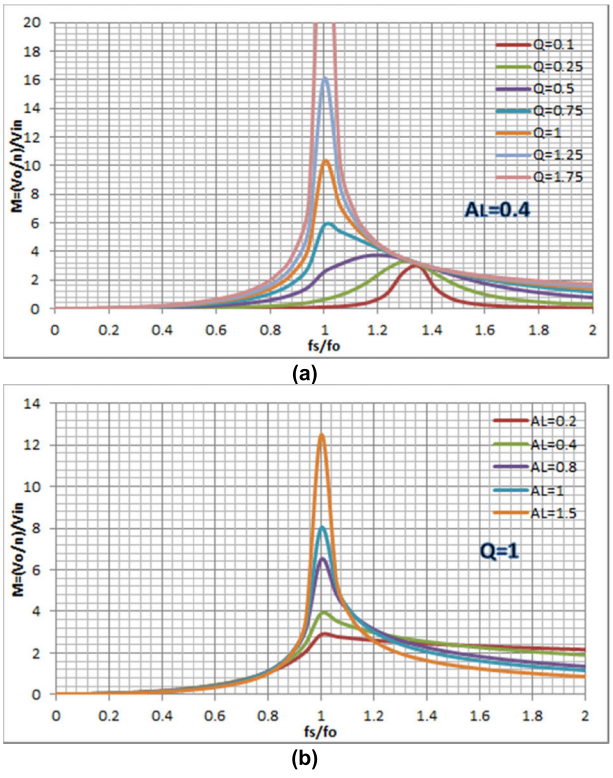

FIGURE 3. Voltage gain versus the relation between switching frequency and resonant frequency for ($0 < f_s/f_r < 2$) characteristics of the proposed LLC converter. (a) Different load factor with $A_L = 0.4$. (b) Different inductance ratios with $Q = 1$.

Substituting (12) into (9), the resonant capacitor is given by:

$$C_r = \frac{1}{L_r \times \omega_r^2} \tag{13}$$

By rearranging (6), utilizing (7)-(11) and taking into account the transformer ratio n, and the gains of both LLC resonant tanks, the voltage gain of the proposed converter as a function of switching frequency f_s, load quality factor Q, and the inductance ratio A_L, can be expressed as

$$M(f_s, Q, A_L) = \frac{\frac{2V_o}{n}}{\bar{V}_{in}} = \frac{2}{\sqrt{(1+A_L)^2\left[1-\left(\frac{f_r}{f_s}\right)^2\right]^2 + \left[\frac{1}{Q}\left(\frac{f_s}{f_r}\frac{A_L}{A_L+1} - \frac{f_r}{f_s}\right)\right]^2}} \tag{14}$$

Based on the relation between the voltage gain and the switching frequency as shown in Fig 3.a, it can be clearly seen that when the switching frequency is lower than the resonant frequency (i.e. $f_s < f_r$), the converter voltage gain drops rapidly as the switching frequency decreases. The converter still can boost the gain for a narrow range as the switching frequency is lower and closer of resonant frequency, and it can be seen there are not much different of gain curves, thus the output voltage cannot be maintained utilizing variable frequency control. While, in case of the switching frequency is lower than half of the resonant frequency, the gain curves reaches nearly zero for all load conditions (i.e. $Q = 0.1$ to $Q = 2$). Therefore, the proposed converter is not suitable for boosting the voltage gain when operating at lower than resonant frequency.

On the other hand, for switching frequency higher than resonant frequency (i.e. $f_s > f_r$), the converter produces significant higher output voltage compared to the input voltage for the whole range of the switching frequency. Furthermore, the gain increases as the switching frequency gets closer to the resonant frequency. This can be seen for wide range of the load (i.e. $Q = 0.25$ to $Q = 2$), where the proposed converter is able to provide voltage gain which is five times higher than the input voltage. For small values of Q (e.g. $Q = 0.1$), the converter can still step up the voltage, but only for a narrow range, when the switching frequency is much higher than resonant frequency. Therefore, the operation range of the proposed converter is selected to be higher than resonant converter to provide high output voltage with wide load variations, where the switching frequency range is (42.5 kHz<f_s<50 kHz). Also, it should be noticed that the A_L value is a fixed design parameter and does not change with operation. According to the gain equation (14), the gain curves have been analyzed with different inductance ratio A_L with constant load factor Q in order to confirm the optimal selection of the suitable A_L value as shown in Fig 3. b. As it can be seen for A_L>1, the gain is much higher than the required gain, as at minimum frequency (42.5 kHz) with taking into account the transformers turns ratios the gain will be much higher than the required gain which is might damage the converter equipment as the devices were selected to achieve 1000 V. While, for values A_L<1, the gain curves are matched with the required voltage gain and the range is suitable to be used for entire selected operation range. Therefore, to ensure safe operation and to satisfy the proposed converter characteristics, the A_L value has been chosen to be 0.4.

For better visual, the three-variable figure of (switching frequency range, fs, load quality factor, Q, and the input voltage) is presented in Figure 4. The expression that completely

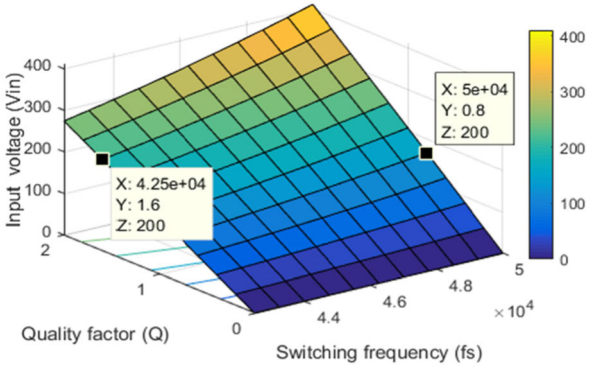

FIGURE 4. The proposed converter voltage gain versus different Q values and switching frequencies.

describes the proposed converter's behaviour can be obtained. To obtain the desired output voltage 1000 V, at minimum switching frequency 42.5 kHz, the load quality factor must be equal to Q = 1.6 whereas to obtain the same output value at the maximum switching frequency 50 kHz, the load is varied to obtain the load quality factor that equal to Q = 0.8 as shown in Fig.4. It is noticed that, to obtain the desired output voltage the input voltage and loading range should be limited to specific values. Therefore, the proposed converter can obtain 1000V by varying the load factor within the range of Q = 0.8 − 1.6, with input voltage V_{in} = 200 V. Moreover, the relation between the input impedance angle and the switching frequency for different Q values is illustrated in Fig. 5. It is seen that the proposed resonant tank impedance is positive which means the proposed tank provides an effective inductive load to the inverter for the all load quality factors (i.e. Q = 0.1 to Q = 2), within the entire operating range (42.5–50 kHz) due to the large selected magnetizing inductance value, Lm. In consequence, the zero crossing of the voltage waveform occurs before the sinusoidal input current waveform. Thus, the primary switches will turn-on at ZVS.

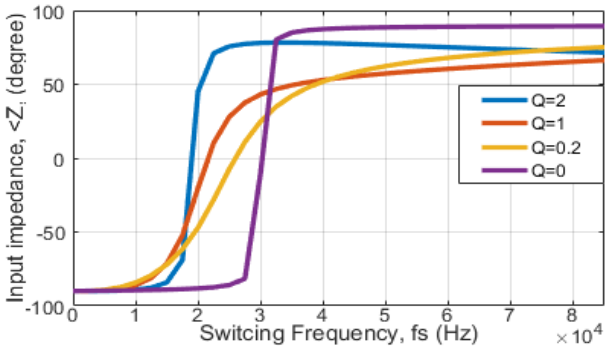

FIGURE 5. The relation between the input impedance angle and the switching frequency for different load quality factors Q.

III. OPERATION PRINCIPLE

The key waveforms of the proposed converter are depicted in Fig. 6, where the ($V_{gs1} - V_{gs6}$) are the driving gate signals of active switches. To ensure the safe operation, a dead time is considered between each two switches in the same leg. The proposed converter has seven operation modes during half switching period and they are described as follows:

Mode 1 [t0–t1, Fig.7a]: This mode starts when switch S_3 is turned off at t = 0, while switches S_2 and S_5 are still on. Here, V_{AB} drops to zero, V_{BC} starts its negative cycle, and V_{CA} is equal to the input voltage. In this mode, $i_{L_{r2}}$ starts to increase and $V_{C_{r2}}$ starts to discharge. Thus, the second resonant tank resonates and makes the freewheeling diode of S_4 to conduct before the end of this mode. The energy stored in the resonant tank is transferred to the output load through the transformer and the rectifier diodes, D_2, and D_3 at the secondary side, as shown Fig 7(a).

Mode 2 [t1–t2, Fig.7b]: The freewheeling diode, S_4 is conducting. This mode will start by turning on S_4 at ZVS.

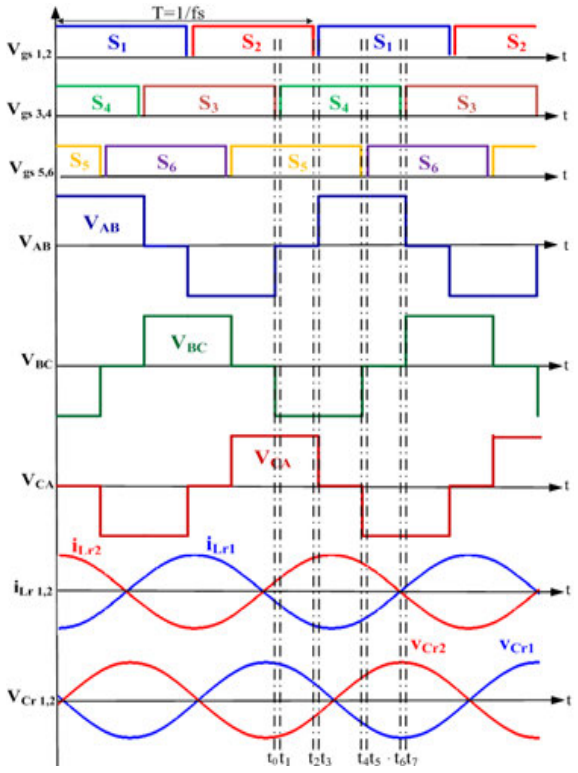

FIGURE 6. The theoretical key waveforms of the proposed converter.

The voltage values, V_{AB}, V_{BC}, and V_{CA} remains the same as mode 1. Also, the resonant inductors are still charging and the capacitors are in discharging operation. The stored energy is transferred to the load through the rectifier diodes, D_2, and D_3.

Mode 3 [t2–t3, Fig.7c]: At the start of this mode, switch S2 is turned off while switches S4 and S5 are still on. The resonant inductors, i_{Lr1}, and i_{Lr2} are almost fully charged, while the capacitors are almost totally discharged. As the stored energy in the resonant inductor must be larger than that of the resonant capacitor to achieve ZVS, the freewheeling diode of the switch S_1 begins to conduct at the end of this mode. Moreover, at the end of this mode, V_{AB} starts its positive cycle to be equal to V_{in}, V_{BC} still remains at same value as the previous mode, and V_{CA} drops to zero. Also, D_2, and D_3 are still conducting to deliver the power to the load.

Mode 4 [t3–t4, Fig.7d]: The conduction of freewheeling diode of switch S_1 enables the switch to turn on at ZVS at the beginning of this mode. In the middle of this mode, both tanks start to resonate by charging the capacitors and discharge the resonant inductors. However, the voltages values, V_{AB}, V_{BC}, and V_{CA} remains the same as the previous mode, and the energy is transferred to the load through D_2, and D_3 of the rectifier.

Mode 5 [t4–t5, Fig.7e]: This mode starts by turning off of switch S5, while switches S_1 and S_4 are still on, which makes V_{AB} equals to V_{in}, V_{BC} to drop to zero, and V_{CA} to start its negative cycle to be equal to $-V_{in}$. Furthermore, the resonant inductors and capacitors will continue the charging and

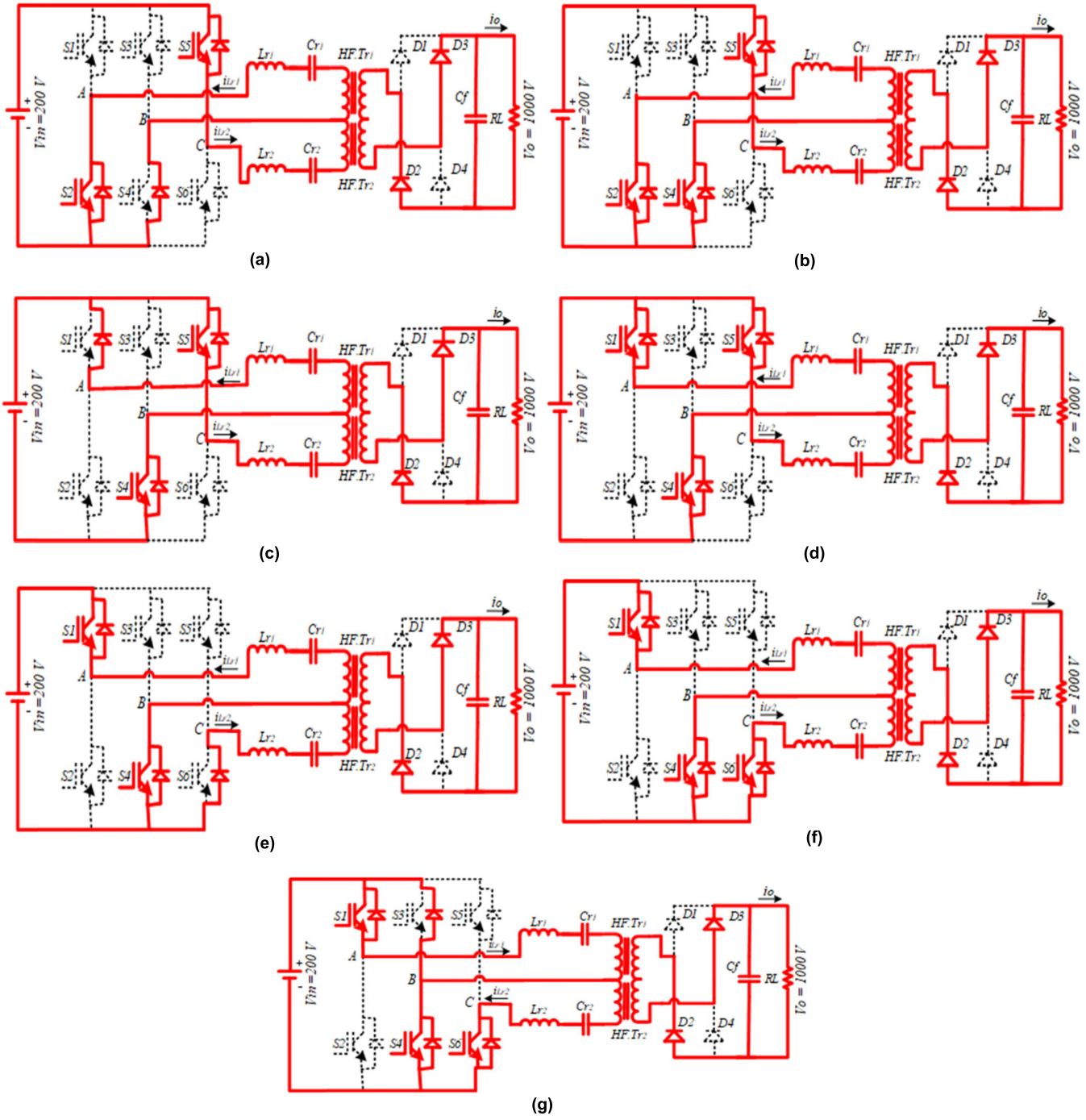

FIGURE 7. Operation modes of the proposed converter. (a) Mode 1. (b) Mode 2. (c) Mode 3. (d) Mode 4. (e) Mode 5. (f) Mode 6. (g) Mode 7.

discharging operations as the previous mode, which leads to the freewheeling diode of S_6 to conduct before this mode ends. The load receives the energy through the rectifier diodes, D_2 and D_3.

Mode 6 [t5–t6, Fig.7f]: As the freewheeling diode of S_6 conducts at the end of the previous mode, this enables S_6 to turn on with a ZVS at the beginning of this mode. Once again, the switches S_1 and S_4 are still on and maintains V_{AB}, V_{BC}, and V_{CA} at the same values as in the previous mode. The resonant inductors are still discharging towards zero at the end of this mode, and the capacitors voltages are increasing to the maximum at the end of this mode. Also, the diode rectifiers, D_2, and D_3 are still conducting to deliver the energy to the load.

Mode 7 [t6–t7, Fig.7g]: At the beginning of this mode switch S_4 is turned off and both tanks starts to resonant by

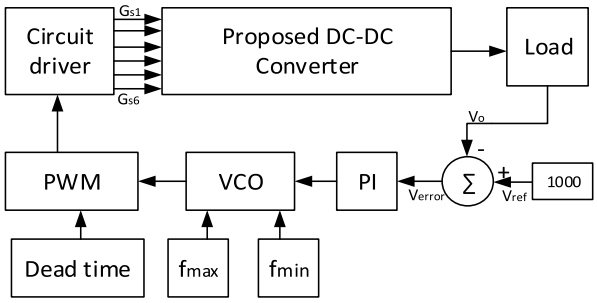

FIGURE 8. The block diagram of the variable frequency control.

charging the inductors and discharging the resonant capacitors. S_1 and S_6 are on in this mode and all V_{AB}, V_{BC}, and V_{CA} are at the same values as previous mode, and the rectifier diodes D_2, and D_3 are conducting. The freewheeling diode of S_3 will conduct at the end of this mode. This repeats the operation where S_3 switches at ZVS and the energy will be transferred to the load via the diodes D_1 and D_4 for next half cycle.

The variable frequency control is applied to the proposed converter to regulate the output voltage by varying the switching frequency. To control the output voltage at a certain level, the switching frequency needs to be selected in accordance to the gain curves shown in Fig. 3.a. In this particular case, to keep the output voltage around 1000V, switching frequency range should be limited to (42.5kHz<f_s<50kHz). Figure 8 depicts the conceptual block diagram of the variable frequency control, where the error signal V_{error} between the measured voltage (output voltage)V_o and the desired voltage (reference voltage) $V_{ref} = 1000\ V$ is processed by a PI controller with ($K_P = 3000, K_i = 0.002$), which are obtained by equations 15, 16 respectively. Therefore, any deviation from the required output based on the error sign, the controller works to increase or decrease the switching frequency in accordance to the desired output voltage. Then the controlled switching signal f_s is applied through PWM to produce controlled switches pulses. Where fixed duty cycle 50%, a dead time of 0.5 μs is considered for all switches ($S_1 - S_6$) for safe operation and ensre ZVS acheavment, with taking into account the phase shift between each leg signals.

$$K_i = L_m \left(\frac{A_L}{L_r - L_m} \right) \times (F_{max} - F_{min}) \times T \quad (15)$$

$$K_p = K_i \times V_{ref} \times \frac{(F_{max} - F_{min})}{2\left(\frac{L_r}{L_m}\right)} \quad (16)$$

where T is a sample time, $T = 1\ \mu s$.

IV. SIMULATION RESULTS

The proposed resonant converter simulation model is built by utilizing Matlab/Simulink software based on the parameters shown in Table 1.

The simulation results clearly shows that the three-phase output inverter voltages (V_{AB}, V_{BC}, V_{CA}), resonant currents ($i_{L_{r1}}$, $i_{L_{r2}}$), and resonant capacitors voltages ($V_{C_{r1}}$, $V_{C_{r2}}$) are

TABLE 1. Prototype specifications.

Parameter	Symbol	Value	Units
Input voltage	V_{in}	200	V
Output voltage	V_o	1000	V
Switching frequency range	f_s	42.5 – 50	kHz
Resonant inductances	$L_{r1} = L_{r2}$	200	µH
Resonant capacitances	$C_{r1} = C_{r2}$	70	µF
Magnetizing inductance	$L_{m1} = L_{m2}$	70	µH
Output capacitance	C_f	470	µF
Rated output power	P_{out}	5000	W
Active Switches	$S_1 - S_6$	IRGP35B60PDPBF	
Transformers ratio	$n_1 = n_2$	0.2	
Microcontroller		TMS320F28335	

balanced as shown in Fig 9. The only difference from the theoretical parts in Fig 6 is that the phase-angel was assumed to be constant based on the average of the selected switching range, which causes a difference in output inverter voltages width and a delay in currents and voltages waveforms. Moreover, the sinusoidal resonant current lags the input voltage for each tank level. This verifies the theoretical part, as the operation region is set to be equal and higher than the resonant frequency (42.5 kHz-50 kHz), Also the selected magnetizing inductance,

L_m enhances the resonant tank to ensure that the tank impedance behaves inductively in the entire operation region. This ensures that all the switches turns-on with ZVS as illustrated in Fig 10.

The performance of the proposed converter is tested for load variation conditions, where the load is stepped down from full load (5 A) to half-load (i.e. 50% of the full-load) at time 0.25s as demonstrated in Fig 11. Furthermore, the performance of the converter with stepped up load from 1 A (i.e. 20% of the full-load) to full load is shown in Fig 12. This confirms the validity of the proposed converter and its controller to maintain the output voltage constant against wide load dynamic variation.

V. EXPERIMENTAL RESULTS

A laboratory prototype of the proposed converter is implemented to experimentally validate the theoretical and simulation outcomes, where the experimental specifications are tabulated in Table 1. The complete experimental configuration of the proposed converter is shown in Fig. 13. Where the experimental setup is divided to two main circuits: power circuit which contains of three-phase inverter supplied by DC voltage source and feeds double stage LLC resonant, then high frequency transformers are connected in series at secondary windings then rectified by full bridge rectifier. Variable resistance conducted as a load by connecting various resistors connected in parallel with through traditional switches to apply load disturbance (load variation).

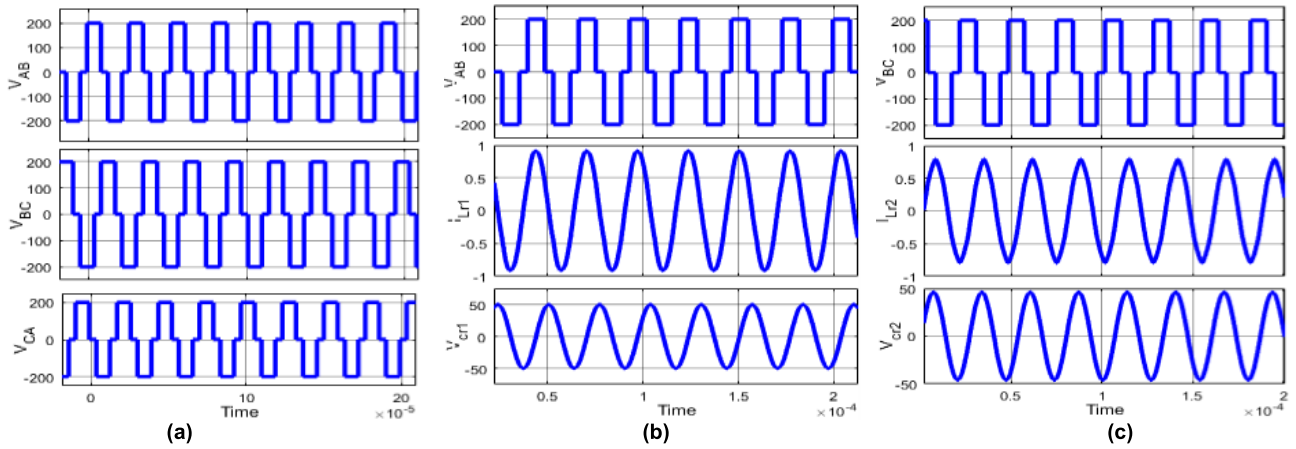

FIGURE 9. Simulation waveforms of the proposed converter (a) three-phase controlled inverter voltages, (b) Resonant tank input voltage V_{AB}, resonant inductor current i_{Lr1}, and resonant capacitor voltage V_{Cr1}, (c) Resonant tank input voltage V_{BC}, resonant inductor current i_{Lr2}, and resonant capacitor voltage V_{Cr2}.

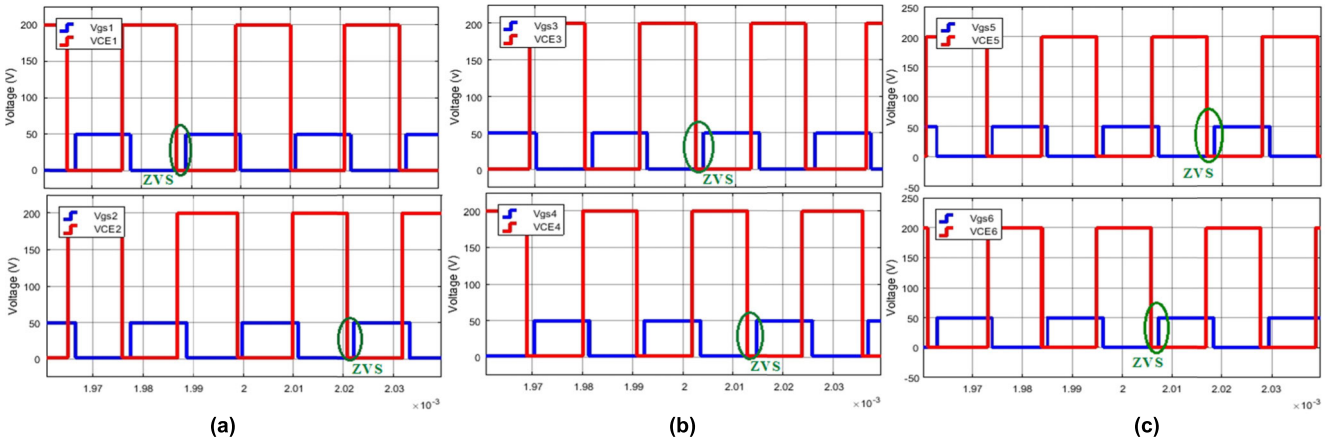

FIGURE 10. Simulation waveforms of gate voltage V_{GE} and collector voltage V_{CE} of all switches (a) switches 1and 2, (b) switches 3 and (c) 4, switches 5 and 6.

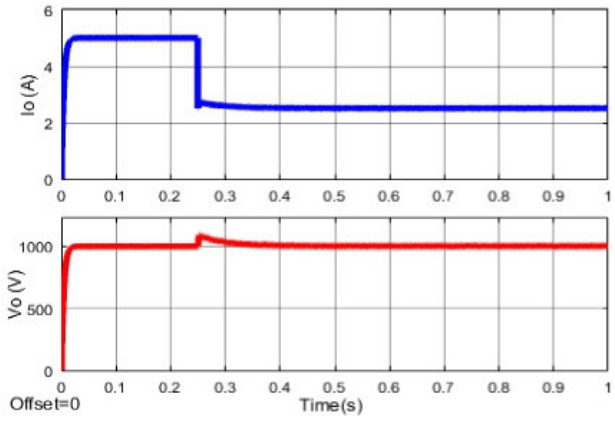

FIGURE 11. Simulation response of the Step-down load condition.

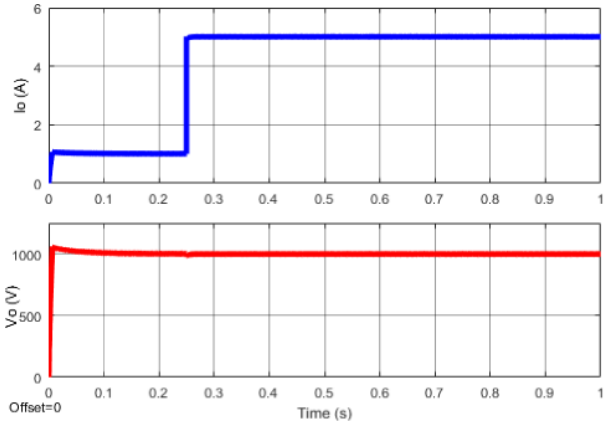

FIGURE 12. Simulation response of the Step-up load condition.

The second circuit is control circuit which contains of voltage sensor which sensing the output voltage and scales down its value, to transform this signal to digital through micro-controller and analog digital converter (ADC). This digital signal is proceeded with variable controller approach by Matlab/Simulink to produce the controlled frequency, which converted to real time switching by the microcontroller to switch the inverter switches.

The three-phase inverter output voltages are shown in Fig 14, where clearly a phase shift is not exactly120 can be easily perceived. This is due to the tanks connections, also the controller as the switching frequency is changing based on

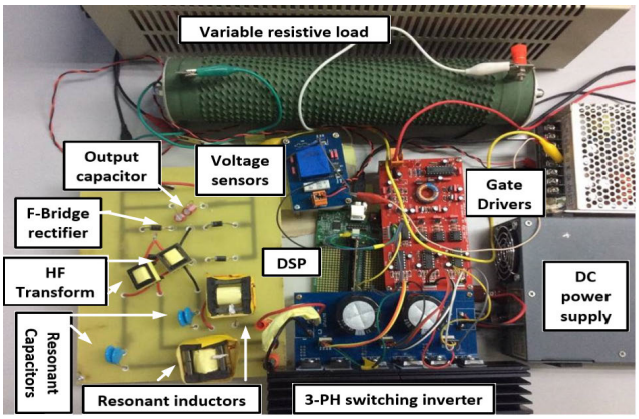

FIGURE 13. Photograph of the experiment set-up of the proposed converter.

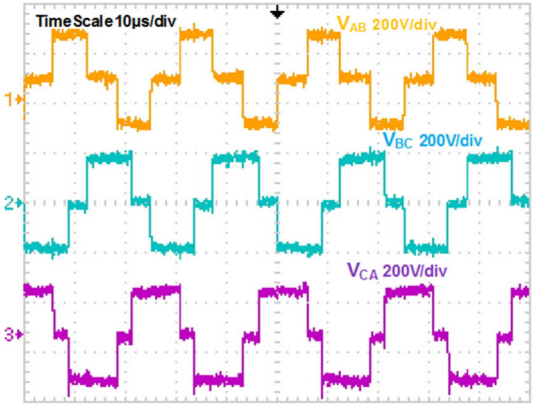

FIGURE 14. Measured waveforms of the three phase controlled Inverter voltages.

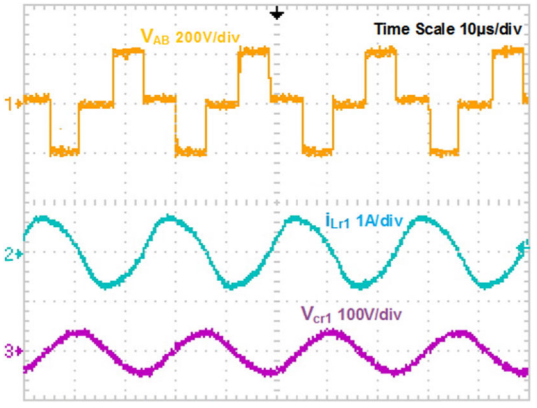

FIGURE 15. Measured experimental results of first resonant tanks waveforms (Resonant tank input voltage V_{AB}, resonant inductor current $i_{L_{r1}}$, and resonant capacitor voltage $V_{C_{r1}}$.) at full load.

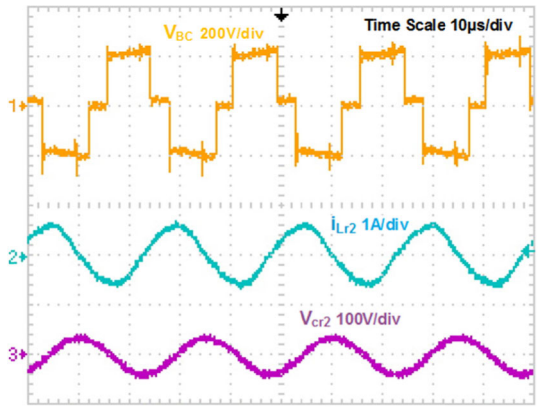

FIGURE 16. Measured experimental results of second resonant tanks waveforms (Resonant tank input voltage V_{BC}, resonant inductor current $i_{L_{r2}}$, and resonant capacitor voltage $V_{C_{r2}}$.) at full load.

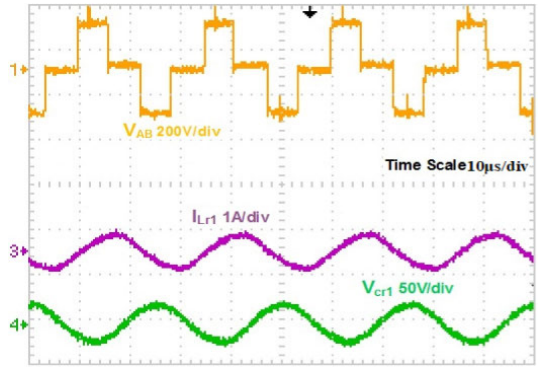

FIGURE 17. Measured experimental results of first resonant tanks waveforms (Resonant tank input voltage V_{AB}, resonant inductor current $i_{L_{r1}}$, and resonant capacitor voltage $V_{C_{r2}}$.) at 20% load.

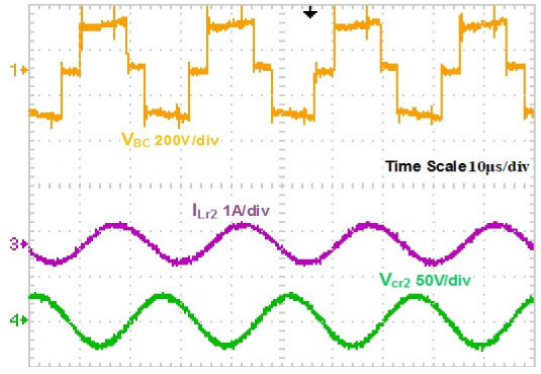

FIGURE 18. Measured experimental results of second resonant tanks waveforms (Resonant tank input voltage V_{BC}, resonant inductor current $i_{L_{r2}}$, and resonant capacitor voltage $V_{C_{r2}}$.) at 20% load.

the output voltage. While the phase shift angle is considered constant within the average of the selected switching range. Additionally, the experimental waveforms of each resonant tank input voltage, resonant current and resonant capacitor voltage at full load condition are measured separately and represented in Figs 15 and 16 respectively. It worth saying that these results are in agreement with simulation results shown in Fig 9 b and 9 c. The difference in voltage width caused from switching frequency variation by controller approach. As the phase angle assumed constant, any variation in frequency from assumed started point will cause width difference that seen in simulation and experimental results. Figs 17 and 18 show the experimental waveforms of each resonant tank at 20% load, and they are in agreement with theoretical and simulation findings as both tanks behaves inductively.

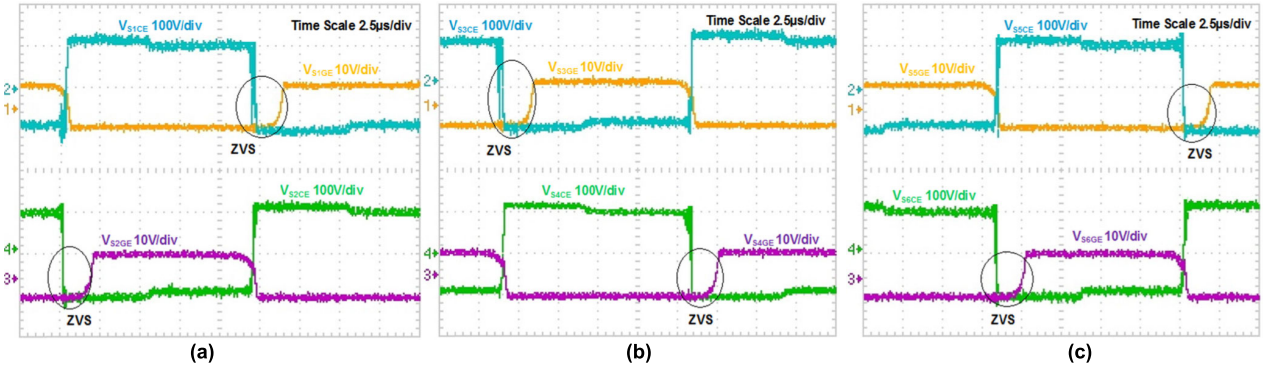

FIGURE 19. *Measured waveforms of the gate voltage V_{GE} and collector voltage V_{CE} for all the switches at* 100% *load (a) S_1, and S_2, (b)S_3, and S_4, (c) S_5, andS_6.*

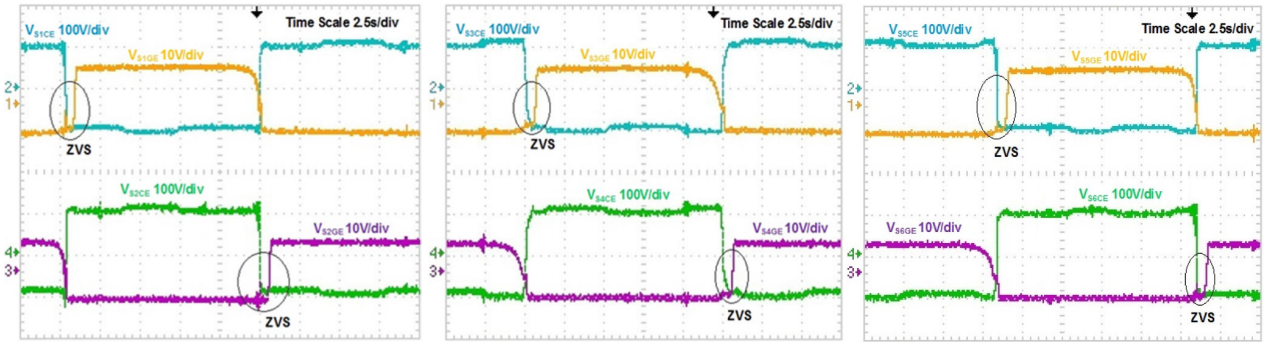

FIGURE 20. *Measured waveforms of the gate voltage V_{GE} and collector voltage V_{CE} for all the switches at* 20% *load (a) S_1, and S_2, (b) S_3, and S_4, (c) S_5, and S_6.*

TABLE 2. Parameters for loss calculation.

Parameter	Symbol	Value	Units
IGBT on-state resistance IGBT	$R_{CE(on)}$	84	mΩ
IGBT turn-off time	t_{off}	110	ns
IGBT's output capacitance	C_{oes}	265	pF
Number of winding turns in each resonant inductor.	N_L	64	turns
Core cross-sectional area	A_C	76	mm^2
Core volume	V_e	5350	mm^3
Core material properties	β	2.7	T
	K_{fe}	68	w/cm^3T^β

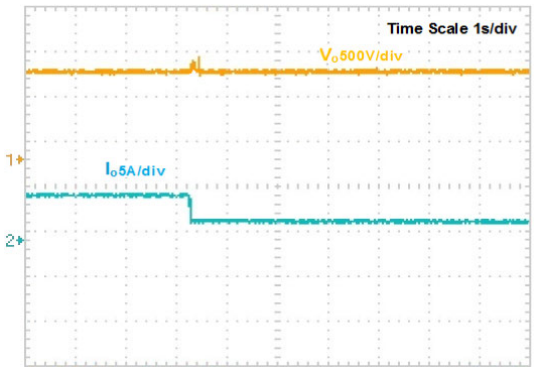

FIGURE 21. Measured results of the output voltage and current for the Step-up load condition.

Furthermore, it is worth noting also that Figs 15, 16, 17 and 18 confirm the ability to achieve ZVS for all switches. The gate voltage and the collector voltage for each switch confirms that the V_{CE} dropped to zero, before the switches were turned on. Thus, all the switches turned on at ZVS for different load conditions as shown in Figs 19 and 20 and this is in agreement with simulation results presented in Fig 10.

The dynamic response of the system is tested through a load step change as represented in Fig. 21, where, the load is changed from 5 kW to 2.5 kW (i.e. corresponding to 200 to 400Ω). Also, the step-up load changes has been applied to change the load from 1 kW to 5 kW (i.e from 20% of the load to full load condition) as demonstrated in Fig. 22. The results confirm that the system has a good response to the load step change, while maintaining the output voltage constant. It should be noted that a small voltage dip was observed during the step up load condition. Even though the undershoot and overshoot voltages occurred in both cases of step-up and step-down load variations, the dynamic system response proved that the system is capable of offering wide load variation

Fig 23 presents the measured efficiency of the proposed converter at different load values and with input voltage of 200V. The maximum efficiency of the proposed converter recorded is 96.2% in the range of operating frequency

TABLE 3. A comparison between the proposed converter and other LLC resonant converters reported in the literature.

Reference	Number of components	Switching frequency, (kHz)	Vin (V)	Vo (v)	Efficiency (%)
[1]	S=8, L=2,T=2, and C=2	180–270	340-400	12	-
[25]	S=12,L=3,T=3, and C=3	34-39	380	300	95.5%
[27]	S=8, L=2,T=2, and C=2	75	410	12	93%
This work	S=6, L=2,T=2, and C=2	42.5-50	200	1000	96.2%

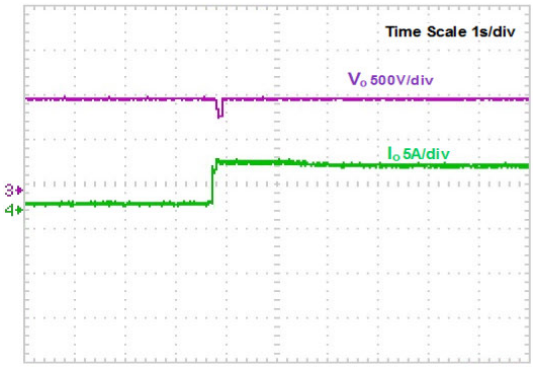

FIGURE 22. Measured results of the output voltage and current for the Step-down load condition.

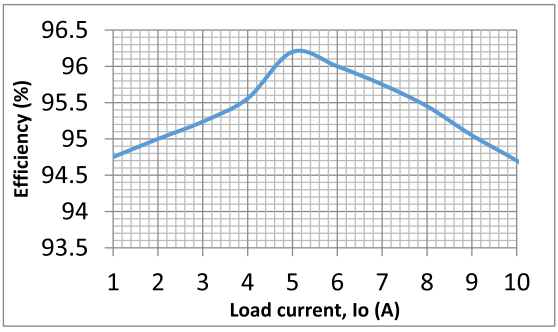

FIGURE 23. Measured efficiency versus output current.

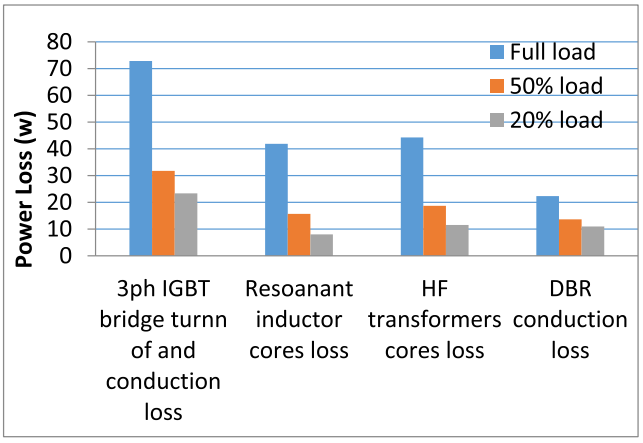

FIGURE 24. Loss breakdown, rated load 50% and 20% load, and Vin = 200V.

and it is considered more efficient compared to three-phase interleaved LLC RC employing the Y-connected rectifier [25]. Fig. 24 depicts the loss breakdown at full load, 50% load, and 20% conditions. The calculations for the losses of individual parts of resonant converters have been studied in details in [28]–[31]. It can be clearly seen that the loss breakdown at 20% load condition is lower than full load condition, which clarifies that the switching, conduction and inductor core losses are notably reduced at load extremes, which are in agreement with the presented results in [28], [29]. The parameters used to calculate the losses are listed in table 2. Due to the reactive power, the reduction of the resonant current is not linearly related to the decrease of the output power, which leads to significant efficiency drop at light load as shown in Fig. 23. Also, it can be noted that the dominant loss of the total losses is the turn-off loss and the conduction loss of the switches. While, the switches are turned on at ZVS, thus the efficiency is notably increased. The efficiency data and the loss breakdown show that the proposed converter should be recommended to be employed in high voltage applications.

Where R_{CE} is the on-state resistance of the IGBT, t_{off} is the is the IGBT turn-off time, C_{oes} IGBT's output capacitance. While, β and K_{fe} represent properties of the used core material, V_e and A_C are the volume and the core cross-section area respectively, and N_L is the number of winding turns in each resonant inductor.

For completeness, the performance of the proposed resonant converter is compared with other LLC resonant DC/DC converters reported in the literature. The proposed converter requires less power switches devices compared to previous converters reported in [1], [25], [27]. Moreover, it is worth noting that only the proposed converter in this paper works as a boost converter with high stepping ratio, while the other topologies can only step-down the voltage, which limits their applications. On the other hand, the analysis of the proposed converter has shown that the converter can provide wide load variation up to 20% to full load. Furthermore, the proposed converter is considered more efficient compared to other reported topology, as the maximum efficiency was 95.5% in [25], while the proposed converter offers nearly 96.2% as shown in Fig. 23. Table 3 summarizes the above comparison.

VI. CONCLUSION

This paper proposed a three phase with two LLC resonant tanks series resonant DC-DC boost converter with variable frequency control. By combining three-phase inverter with two LLC resonant tanks, and both tanks are sharing a full bridge diode rectifier, both tanks are assumed to be identical to ensure balanced resonant tank variables. In addition, to produce equal resonant frequencies to simplify the design considerations, which provided the following characteristics: 1) compared to conventional three interleaved LLC resonant converter, the proposed converter could reduce the number of power switches, which has a significant impact on reducing the weight, cost, and the circuit simplicity. 2) The output voltage of the proposed converter is five times larger than input voltage, which means that the proposed converter is suitable for high voltage applications. 3) The variable switching frequency control was adopted and maintained a wide load variation for the proposed converter. This confirms the theoretical analysis of the converter that the gain is not strictly affected by the load factor as it relies heavily on the ratio of switching to resonant frequency. The laboratory prototype has verified the system performance and has proven the effectiveness of the theoretical parts.

REFERENCES

[1] H. Wang, Y. Chen, Y.-F. Liu, J. Afsharian, and Z. Yang, "A passive current sharing method with common inductor multiphase LLC resonant converter," *IEEE Trans. Power Electron.*, vol. 32, no. 9, pp. 6994–7010, Sep. 2017.

[2] H. Wu, Y. Lu, T. Mu, and Y. Xing, "A family of soft-switching DC–DC converters based on a phase-shift-controlled active boost rectifier," *IEEE Trans. Power Electron.*, vol. 30, no. 2, pp. 657–667, Feb. 2015.

[3] M. T. Outeiro, R. Visintini, and G. Buja, "Considerations in designing power supplies for particle accelerators," in *Proc. 39th IEEE Annu. Conf. Ind. Electron. Soc. (IECON)*, Nov. 2013, pp. 7076–7081.

[4] M. Salem, A. Jusoh, N. R. N. Idris, H. Das, and I. Alhamrouni, "Resonant power converters with respect to passive storage (LC) elements and control techniques—An overview," *Renew. Sustain. Energy Rev.*, vol. 91, pp. 504–520, Aug. 2018.

[5] M. T. Outeiro, G. Buja, and D. Czarkowski, "Resonant power converters: An overview with multiple elements in the resonant tank network," *IEEE Ind. Electron. Mag.*, vol. 10, no. 2, pp. 21–45, Jun. 2016.

[6] M. Salem, A. Jusoh, N. R. N. Idris, and I. Alhamrouni, "Comparison of LCL resonant converter with fixed frequency, and variable frequency controllers," in *Proc. IEEE Conf. Energy Convers. (CENCON)*, Oct. 2017, pp. 84–89.

[7] M. T. Outeiro and G. Buja, "Comparison of resonant power converters with two, three, and four energy storage elements," in *Proc. 41st IEEE Annu. Conf. Ind. Electron. Soc. (IECON)*, Nov. 2015, pp. 001406–001411.

[8] W. Sun and X. Ge, "DC-link stability and modeling of inverter-IM vector control system based on LTP theory," in *Proc. 22nd Int. Conf. Elect. Mach. Syst. (ICEMS)*, Aug. 2019, pp. 1–5.

[9] C.-H. Chien, Y.-H. Wang, and B.-R. Lin, "Series resonant converter with series-parallel transformers for high input voltage applications," in *Proc. IEEE Region 10 Conf. (TENCON)*, Nov. 2011, pp. 873–877.

[10] X. Xie, J. Zhang, C. Zhao, Z. Zhao, and Z. Qian, "Analysis and optimization of LLC resonant converter with a novel over-current protection circuit," *IEEE Trans. Power Electron.*, vol. 22, no. 2, pp. 435–443, Mar. 2007.

[11] M. Salem, V. K. Ramachandaramurthy, P. Sanjeevikumar, Z. Leonowicz, and V. Yaramasu, "Full bridge LLC resonant three-phase interleaved multi converter for HV applications," in *Proc. IEEE Int. Conf. Environ. Elect. Eng., IEEE Ind. Commercial Power Syst. Eur. (EEEIC/I CPS Eur.)*, Jun. 2019, pp. 1–6.

[12] B.-R. Lin and S.-F. Wu, "ZVS resonant converter with series-connected transformers," *IEEE Trans. Ind. Electron.*, vol. 58, no. 8, pp. 3547–3554, Aug. 2011.

[13] I. Alhamrouni, M. R. B. Hamzah, M. Salem, A. Jusoh, A. B. Khairuddin, and T. Sutikno, "A bidirectional resonant converter based on wide input range and high efficiency for photovoltaic application," *Int. J. Power Electron. Drive Syst.*, vol. 10, no. 3, pp. 1469–1475, 2019.

[14] C.-H. Chang, C.-A. Cheng, and H.-L. Cheng, "Modeling and design of the LLC resonant converter used as a solar-array simulator," *IEEE J. Emerg. Sel. Topics Power Electron.*, vol. 2, no. 4, pp. 833–841, Dec. 2014.

[15] J. Deng, S. Li, S. Hu, C. C. Mi, and R. Ma, "Design methodology of LLC resonant converters for electric vehicle battery chargers," *IEEE Trans. Veh. Technol.*, vol. 63, no. 4, pp. 1581–1592, May 2014.

[16] F. Musavi, M. Craciun, D. S. Gautam, and W. Eberle, "Control strategies for wide output voltage range LLC resonant DC–DC converters in battery chargers," *IEEE Trans. Veh. Technol.*, vol. 63, no. 3, pp. 1117–1125, Jan. 2014.

[17] M. Salem, A. Jusoh, N. R. Nik Idris, T. Sutikno, and Y. Buswig, "Phase-shifted series resonant converter with zero voltage switching turn-on and variable frequency control," *Int. J. Power Electron. Drive Syst.*, vol. 8, no. 3, p. 1184, Jan. 2018.

[18] G. Liu, Y. Jang, M. M. Jovanovi, and J. Q. Zhang, "Implementation of a 3.3-kW DC–DC converter for EV on-board charger employing the series-resonant converter with reduced-frequency-range control," *IEEE Trans. Power Electron.*, vol. 32, no. 6, pp. 4168–4184, Jun. 2017.

[19] I. O. Lee and G. W. Moon, "Three-level LLC SRC for high and wide input voltage applications," in *Proc. 8th Int. Conf. Power Electron. (ECCE Asia)*, 2011, pp. 52–59.

[20] M. Malinowski, K. Gopakumar, J. Rodriguez, and M. A. Pérez, "A survey on cascaded multilevel inverters," *IEEE Trans. Ind. Electron.*, vol. 57, no. 7, pp. 2197–2206, Jul. 2010.

[21] B.-R. Lin and Y.-B. Nian, "Analysis and implementation of a new three-level converter," *J. Power Electron.*, vol. 14, no. 3, pp. 478–487, May 2014.

[22] F. Liu, Y. Chen, and X. Chen, "Comprehensive analysis of three-phase three-level LC-type resonant dc/dc converter with variable frequency control—Series resonant converter," *IEEE Trans. Power Electron.*, vol. 32, no. 7, pp. 5122–5131, Sep. 2016.

[23] F. Liu, G. Hu, and X. Ruan, "Three-phase three-level DC/DC converter for high input voltage and high power applications-adopting symmetrical duty cycle control," *IEEE Trans. Power Electron.*, vol. 29, no. 1, pp. 56–65, Jan. 2014.

[24] J. Rabkowski, D. Peftitsis, and H.-P. Nee, "Parallel-operation of discrete SiC BJTs in a 6-kW/250-kHz DC/DC boost converter," *IEEE Trans. Power Electron.*, vol. 29, no. 5, pp. 2482–2491, May 2014.

[25] H.-S. Kim, J.-W. Baek, M.-H. Ryu, J.-H. Kim, and J.-H. Jung, "The high-efficiency isolated AC–DC converter using the three-phase interleaved LLC resonant converter employing the Y-connected rectifier," *IEEE Trans. Power Electron.*, vol. 29, no. 8, pp. 4017–4028, Nov. 2014.

[26] Z. Guo, D. Sha, and X. Liao, "Hybrid phase-shift-controlled three-level and *LLC* DC–DC converter with active connection at the secondary side," *IEEE Trans. Power Electron.*, vol. 30, no. 6, pp. 2985–2996, Jun. 2015.

[27] K.-H. Yi and G.-W. Moon, "Novel two-phase interleaved LLC series-resonant converter using a phase of the resonant capacitor," *IEEE Trans. Ind. Electron.*, vol. 56, no. 5, pp. 1815–1819, May 2009.

[28] S. Zong, H. Luo, W. Li, Y. Deng, and X. He, "Asymmetrical duty cycle-controlled *LLC* resonant converter with equivalent switching frequency doubler," *IEEE Trans. Power Electron.*, vol. 31, no. 7, pp. 4963–4973, Jul. 2016.

[29] U. Kundu, K. Yenduri, and P. Sensarma, "Accurate ZVS analysis for magnetic design and efficiency improvement of full-bridge LLC resonant converter," *IEEE Trans. Power Electron.*, vol. 32, no. 3, pp. 1703–1706, Mar. 2017.

[30] R. Yu, G. K. Y. Ho, B. M. H. Pong, B. W.-K. Ling, and J. Lam, "Computer-aided design and optimization of high-efficiency LLC series resonant converter," *IEEE Trans. Power Electron.*, vol. 27, no. 7, pp. 3243–3256, Jul. 2012.
[31] J. Lu, D. J. Perreault, and K. K. Afridi, "Impedance control network resonant DC-DC converter for wide-range high-efficiency operation," in *Proc. IEEE Appl. Power Electron. Conf. Expo. (APEC)*, Mar. 2015, pp. 1440–1447.

MOHAMED SALEM (Member, IEEE) received the B.Eng. degree in electrical and power engineering from Elmergib University, Al Khums, Libya, in 2008, the M.Sc. degree in electrical engineering from the Tun Hussein Onn University of Malaysia (UTHM), Batu Pahat, Johor, Malaysia, in 2011, the Ph.D. degree from the Department of Power Engineering, Faculty of Electrical Engineering, Universiti Teknologi Malaysia (UTM), Malaysia, in August 2017. He has been a Senior Lecturer with the School of Electrical and Electronic Engineering, Universiti Sains Malaysia (USM), Penang, Malaysia, since July 2018. He has authored and coauthored number of well recognized journals and conference papers. His research interests are in DC–DC converter, renewable energy applications, energy conversion, and the control of power electronics systems. He is a registered Graduate Engineer, Malaysia (BEM) in the electrical track.

VIGNA K. RAMACHANDARAMURTHY (Senior Member, IEEE) received the Ph.D. degree in electrical engineering from the University of Manchester Institute of Science and Technology (UMIST), in 2001. He is currently a Professor with the Institute of Power Engineering, Universiti Tenaga Nasional. He has completed more than 200 projects in renewable energy. He has also developed several technical guidelines for distributed generation in Malaysia. He is the Principal Consultant for Malaysia's biggest electrical utility and Tenaga Nasional Berhad. His areas of interests include power systems related studies, renewable energy, energy storage, power quality, electric vehicle, and rural electrification. In 2008, he received the IET Mike Sargeant Award for career achievement. In 2009, he received the Institution of Engineers Malaysia (IEM) Young Engineers Award. He has served as the IET Malaysia Chairman, IET Council Member, Institution of Engineers Malaysia (IEM) Council Member, and IET Younger Members Board representing West Asia, International Professional Registration Advisor, an Interviewer and a Convenor for Chartered Engineering (UK) in Malaysia. He is also a Chartered Engineer registered with the Engineering Council, U.K., and a Professional Engineer registered with the Board of Engineers Malaysia.

AWANG JUSOH was born in Terengganu, Malaysia, in 1964. He received the B.Eng. degree from Brighton Polytechnic, U.K., in 1988, and the M.Sc. and Ph.D. degrees from the University of Birmingham, U.K., in1995 and 2004, respectively. He is currently an Associate Professor with the Department of Power Engineering, Faculty of Electrical Engineering, University Technology Malaysia (UTM), Johor, Malaysia. His research interests are in DC–DC converter, renewable energy, and the control of power electronics systems.

SANJEEVIKUMAR PADMANABAN (Senior Member, IEEE) received the bachelor's degree in electrical engineering from the University of Madras, India, in 2002, the master's degree (Hons.) in electrical engineering from Pondicherry University, India, in 2006, and the Ph.D. degree in electrical engineering from the University of Bologna, Italy, in 2012.

He was an Associate Professor with VIT University, from 2012 to 2013. In 2013, he joined the National Institute of Technology, India, as a Faculty Member. In 2014, he was invited as a Visiting Researcher with the Department of Electrical Engineering, Qatar University, Qatar, funded by the Qatar National Research Foundation (Government of Qatar). He continued his research activities with the Dublin Institute of Technology, Ireland, in 2014. He was an Associate Professor with the Department of Electrical and Electronics Engineering, University of Johannesburg, South Africa, from 2016 to 2018. Since 2018, he has been a Faculty Member of the Department of Energy Technology, Aalborg University, Esbjerg, Denmark. He has authored over 300 scientific articles. He is a Fellow of the Institution of Engineers, India, the Institution of Electronics and Telecommunication Engineers, India, and the Institution of Engineering and Technology, U.K. He was a recipient of the Best Paper cum Most Excellence Research Paper Award from the IET-SEISCON'13, IET-CEAT'16, IEEE-EECSI'19, and IEEE-CENCON'19, as well as five best paper awards from ETAEERE'16 sponsored *Lecture Notes in Electrical Engineering* (Springer). He is an Editor/Associate Editor/Editorial Board for refereed journals, in particular, the IEEE Systems Journal, IEEE Access, the *IET Power Electronics*, and the *Journal of Power Electronics* (South Korea), as well as the Subject Editor of the *IET Renewable Power Generation*, the *IET Generation, Transmission and Distribution*, and *FACTS journal* (Canada).

MOHAMAD KAMAROL (Senior Member, IEEE) received the B.Eng. degree (Hons.) in electrical engineering from Universiti Technology Mara, Malaysia, in 2000, the M.Eng. degree from the Kyushu Institute of Technology, Japan, in 2005, and the D.Eng. degree, in 2008. Within the Ph.D. course, he received the Chatterton Young Investigator Award from the IEEE International Symposia on Discharges and Electrical Insulation in Vacuum, in 2006. In 2002, he joined Universiti Sains Malaysia (USM) with a University ASTS Fellowship; later on, has been a Senior Lecturer, in 2008; and was promoted to an Associate Professor, in 2014. He was a Senior Engineer with Sankyo Seiki (M) Sdn. Bhd., for almost eight years. He was a Visiting Researcher with the High Voltage Laboratory, Kyushu Institute of Technology, Japan, from 2013 to 2014. His research interests include the insulation properties in oil palm, solid dielectric material, insulation properties of environmentally benign gas, and PD detection technique for insulation diagnosis of power apparatus and electrical machine. He is also involved in temperature rise and short-circuit electromagnetic study of busbar systems and HVDC systems. He is a member of the IET, the Board of Engineering Malaysia, and the Institute Engineering Malaysia. He is a Professional Engineer and a Chartered Engineer.

JIASHEN TEH (Member, IEEE) received the B.Eng. degree (Hons.) in electrical and electronic engineering from Universiti Tenaga Nasional (UNITEN), Selangor, Malaysia, in 2010, and the Ph.D. degree in electrical and electronic engineering from The University of Manchester, Manchester, U.K., in 2016. Since 2016, he has been a Senior Lecturer/Assistant Professor with Universiti Sains Malaysia (USM), Penang, Malaysia. In 2018, he was appointed and served as an Adjunct Professor with the Green Energy Electronic Center, National Taipei University of Technology (Taipei Tech), Taipei, Taiwan. In 2019, he joined the Intelligent Electric Vehicle & Green Energy Center, National Chung Hsing University (NCHU), Taichung, Taiwan, where he is currently an Adjunct Professor. His research interests include the probabilistic modeling of power systems, grid-integration of renewable energy sources, and reliability modeling of smart grid networks. He is a Chartered Engineer (CEng) conferred by the Engineering Council, U.K., and The Institution of Engineering and Technology (IET), a member of the IEEE Power and Energy Society, The Institution of Engineers Malaysia (IEM), and a registered Engineer in the Board of Engineers Malaysia (BEM). He received the outstanding publication awards from USM, in 2017 and 2018. He is also a regular invited Reviewer of the *International Journal of Electrical Power and Energy Systems*, IEEE Access, the IEEE Transactions on Reliability, the IEEE Transactions on Industrial Electronics, and the *IET Generation, Transmission and Distribution*.

DAHAMAN ISHAK (Senior Member, IEEE) received the B.Sc. degree in electrical engineering from Syracuse University, Syracuse, NY, USA, in 1990, the M.Sc. degree in electrical power from Newcastle University, Newcastle upon Tyne, U.K., in 2001, and the Ph.D. degree in electrical engineering from the University of Sheffield, Sheffield, U.K., in 2005. He is currently an Associate Professor with the School of Electrical and Electronic Engineering, Universiti Sains Malaysia, Penang, Malaysia. His research interests include electrical machines and drives, power electronic converters, and renewable energy.